References and Notes

1. T. E. Green and C. N. Hinshelwood, *J. Chem. Soc. (Lond.)* (1926), p. 1709; C. S. Howard and F. Daniels, *J. Phys. Chem.* **62**, 360 (1958); J. M. Fraser and F. Daniels, *ibid.*, p. 215; E. R. S. Winter, *J. Catal.* **22**, 158 (1971); M. Shelef, K. Otto, H. Ghandi, *Atmos. Environ.* **3**, 107 (1969); S. W. Harris, E. F. Morello, G. H. Peters, U.S. Patent No. 3,459,494.
2. P. R. Ryason and J. Harkins, *J. Air Pollut. Control Assoc.* **17**, 796 (1967); H. C. Andersen, W. J. Green, D. R. Steele, *Ind. Eng. Chem.* **53**, 199 (1971); K. Otto and M. Shelef, *J. Phys. Chem.* **76**, 37 (1972); R. J. H. Voorhoeve, J. P. Remeika, D. W. Johnson, Jr., *Science* **180**, 62 (1973); J. Cohn, D. R. Steele, H. C. Anderson, U.S. Patent No. 2,975,025.
3. R. Cramer, *J. Am. Chem. Soc.* **87**, 4717 (1965).
4. W. B. Hughes, *Chem. Commun.* (1969), p. 1126.
5. B. R. James and G. L. Rempel, *ibid.* (1967), p. 158.
6. Supported by NSF grant GP-40088X. R.E. is an Alfred P. Sloan Foundation Fellow, 1972 to 1974.

8 January 1974

Air Pollution: Remote Detection of Several Pollutant Gases with a Laser Heterodyne Radiometer

Abstract. *An infrared heterodyne radiometer with a spectral resolution of 0.04 reciprocal centimeters has been used to remotely detect samples of ozone, sulfur dioxide, ammonia, and ethylene at room temperature, and samples of nitric oxide at 390K. Each gas was observed in a background of nitrogen or oxygen at atmospheric pressure. Sensitivities to some of these gases are adequate for detection of ambient concentrations as low as a few parts per billion.*

A heterodyne radiometer, with a CO_2 laser as a local oscillator, has been used to remotely detect several laboratory samples of gaseous pollutants at ambient temperature. The radiometer is a passive device, sensitive to the characteristic thermal radiation from each gas. Previous demonstrations of heterodyne radiometer sensitivities to SO_2 and CO_2 were accomplished by heating the gas samples (*1*). The sensitivities to O_3, NH_3, and CH_4 were found to be adequate for detection of ambient concentrations in the parts per billion (ppb) region. The sensitivities to SO_2 are on the border line for detection of ambient concentrations around 50 ppb, and it may be possible to improve this by a factor of 4 if detection wavelengths near 8.8 μm are used instead of our operating region around 9.0 μm. A CO laser, operating near 5.2 μm, has also been used as a local oscillator in the detection of nitric oxide (NO) at a temperature of 390 K. The passive heterodyne radiometer does not appear to be capable of detecting ambient NO at normal smog concentrations; however, it can be used to monitor NO concentrations in stationary source emissions which are at elevated temperatures.

The heterodyne radiometer is useful for remote observation and measurement of atmospheric constituents whenever high spectral resolution is desired. The spectral resolution makes the instrument very selective, as interference problems due to overlapping lines or bands are minimized. Possible applications include monitoring of local air pollution from the ground or of global atmospheric quality from spacecraft. There are also several applications in infrared astronomy. Applications to remote sensing of atmospheric pollutants have been discussed in connection with infrared tunable diode lasers (*2*) and infrared gas lasers (*3*).

The heart of the instrument consists of an infrared laser as a local oscillator, and a high-speed infrared detector. The local oscillator beam and the radiation to be detected are normally combined via a beam splitter and are then focused onto the detector, which acts as a mixer. The instrument is sensitive to a narrow (by infrared standards) band of beat frequencies on each side of the local oscillator frequency. The sensitive bandwidth is determined by the frequency responses of the infrared detector and the intermediate frequency (IF) amplification chain which follows the detector. Since the size of the mixing signal increases as the local oscillator power increases, the ultimate sensitivity is reached when local oscillator fluctuations become the chief source of noise. If a Dicke-type radiometer configuration is used, and the only local oscillator fluctuations are due to quantum fluctuations, then the signal-to-noise ratio (S/N) when the radiometer is looking at a radiating slab of gas at temperature T with emissivity $\epsilon(\nu)$ is

$$\frac{S}{N}=\frac{1}{4}\,\frac{\eta\,(\tau/B)^{1/2}}{\exp\left(\frac{h\nu}{kT}\right)-1}\int_{\nu_{LO}-B}^{\nu_{LO}+B}\epsilon(\nu)d\nu \qquad (1)$$

(*1*). In this expression η is the quantum efficiency of the infrared mixer (about 0.5 in our case), ν_{LO} is the local oscillator frequency, B is the IF bandwidth, and τ is the integration time after the IF detection process. In practice, the frequencies of IF amplification range from a few to several hundred megahertz. Thus, the integration range in Eq. 1 is not strictly correct, but it is a good approximation.

Although the frequency-dependent expression $[\exp(h\nu/kT)-1]^{-1}$ in Eq. 1 varies slowly enough to be placed outside the integral, it produces a large effect in values of S/N for radiometer operation at various infrared wavelengths. As we see in Fig. 1, this causes the heterodyne radiometer to be much more sensitive to radiating gases when operating at longer wavelengths in the infrared. Thus, at room temperature the sensitivity to gases that radiate in the wavelength region above 9 μm is much better than the sensitivity to NO, which radiates in the region from 5.0 to 5.5 μm.

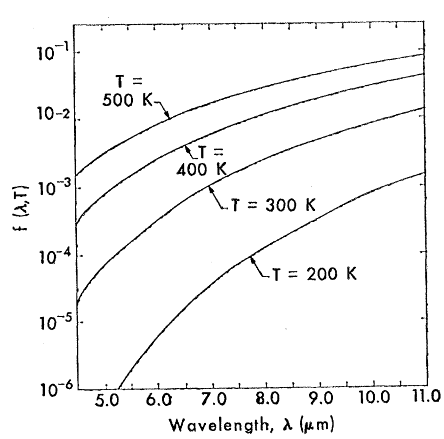

Fig. 1. Wavelength dependence of the sensitivity of the heterodyne radiometer. The function plotted is $f(\lambda,\ T)=[\exp(hc/\lambda kT)-1]^{-1}$; $\nu=c/\lambda$ where c is the velocity of light. (See Eq. 1 in text.) The temperatures indicated here are those of the gases within the radiometer's field of view.

In our experiments, a CO_2 laser was used to provide emission frequencies which overlapped emission lines of SO_2, O_3, C_2H_4, and NH_3. A CO laser, cooled with a Dry Ice–methanol closed cycle system, was used to provide a local oscillator line which overlapped an NO emission line. Both lasers were sealed off and had very stable frequencies. Each laser could be tuned over a large number of lines by adjusting a diffraction grating at one end of the cavity. Sodium chloride optics were used to combine the local oscillator and thermal radiation signals, and focus them onto a high-speed germanium photoconductor doped with copper. The mixer was roughly 0.3 by 0.4 by 3.5 mm. The cross-sectional dimensions were made small in order to reduce the capacitance and operating resistance of the mixer. When a local oscillator power of 40 mw was incident on the mixer, the d-c resistance dropped to about 2000 ohms. The beat frequencies between 10 and 600 Mhz were amplified by 50-ohm input IF amplifiers. When a bias power of 30 to 40 mw was applied across the mixer, the quantum noise induced by the local oscillator was enough to raise the total noise level to 3 to 5 db above that of the IF amplifier over the frequency region of interest. We normally operated the radiometer under these conditions.

The gases to be detected were individually placed inside a cell 15 cm long. When NO, SO_2, C_2H_4, and NH_3 were detected, small amounts were leaked into the cell, and then the cell pressure was brought up to atmospheric pressure by adding N_2. When the mixture of NO and N_2 was used, the cell was heated to 390 K beforehand. A mixture of O_3 and O_2 was used in the cell for detection of O_3. To achieve the Dicke radiometer configuration (*4*), a reflecting chopper was used to allow the receiver to alternately view the gas cell and a cold black surface inside a small, liquid nitrogen Dewar. A mirror placed behind the gas cell directed the field of view to the same cold reference surface. A radio-frequency detector demodulated the resulting IF signal, and the output was fed into a phase-lock detector.

The sensitivities to the various gases are shown in Table 1. The minimum detectable amounts in the second column (in units of concentration times path length give a signal-to-noise ratio of one when a time constant, τ, of 10 seconds is used. For these measurements, $B = 600$ Mhz. This corresponds to a spectral resolution of 0.04 cm^{-1}. Greater sensitivity can be achieved by increasing the product $B\tau$, or by putting an antireflection coating on the mixer. The latter step could improve the sensitivity by nearly a factor of 2. The NO emission line which was observed in these experiments is the $R(31/2)_{3/2}$ line. An overlap between the 9–8, $P(9)$ line of the CO laser and the stronger $R(13/2)_{1/2}$ line of NO can be used to increase sensitivity to NO. The ratio of absorption coefficients for these two NO lines is nearly 5 at 300 K and 2.6 at 400 K. The $^{12}C^{18}O_2$ laser overlaps the upper end of the ν_1 band of SO_2 and a better overlap with SO_2 should be possible near 8.8 μm. A PbSnTe diode laser might be used as a local oscillator in this region. At present, it is very difficult to satisfy all the local oscillator requirements (frequency and amplitude stability, and several milliwatts of single mode output power) with a diode laser. However, improvements in diode laser technology should make them useful for this application in the future.

The passive heterodyne radiometer can be used to monitor atmospheric pollutants in several modes. A ground-based instrument in an upward looking mode can detect thermal radiation from gas molecules directly, or it can detect absorption lines while looking at the sun. [Some applications of solar heterodyne radiometry have been discussed by McElroy (*5*).] If the pollutants of interest are uniformly mixed under an inversion layer at an altitude of a few kilometers, very good sensitivities can be obtained. For example, using Table 1 we compute the minimum detectable concentration of O_3 under an inversion layer at 1 km as 2 ppb. A downward looking heterodyne radiometer in an aircraft or spacecraft can be used to detect various constituents by monitoring absorption lines in the earth's 300 K blackbody spectrum. This technique is sensitive to gases at upper altitudes, which are in cold regions of the atmosphere, but not very useful for detection of pollutants at low altitudes, which are near the temperature of the earth's surface. The aircraft instrument can also monitor constituents in the upper atmosphere by observing absorption lines in the solar spectrum. Since the forte of the heterodyne radiometer is its high spectral resolution, it should be particularly useful in upper altitude monitoring, where line widths are much narrower. Some applications of heterodyne radiometry to atmospheric and jet wake monitoring in the stratosphere and upper troposphere have been studied recently (*6*). Emissions from stationary sources can be monitored from remote locations: the inherent specificity would reduce difficulties caused by the presence of heavy concentrations of water vapor and CO_2. The field of view of the heterodyne radiometer can be made very small without reducing the signal-to-noise ratio. This would permit observations from large distances, where active sensing techniques might fail due to lack of sensitivity.

Accurate atmospheric measurements with the heterodyne radiometer requires operation at a minimum of two local oscillator wavelengths in order to eliminate the effects of broad-band interfering species such as water vapor. If a tunable diode local oscillator is used, frequency-modulated tuning might be used instead. Water vapor absorption is a particular nuisance around the 5.2-μm NO absorption band, although near the two NO lines which we have mentioned as useful for observation, water vapor absorption is relatively weak. It is important to have complete knowledge of absorption and thermal emission due to interfering species near the local oscillator wavelengths.

Atmospheric turbulence can degrade the sensitivity of the heterodyne radiometer in some applications, but proper instrument design can minimize these effects. Turbulence will degrade the phase fronts of radiation traveling from a source to the radiometer, which can reduce the heterodyne mixing efficiency. However, an analysis of this effect indicates that, for radiometers operating in the wavelength region above 5 μm, collecting aperture diameters can be made as large as 1 m with very little loss in heterodyne efficiency over a range of several kilometers (*7*). If the source covers a small solid angle, turbulence can steer the instrument's field of view off the source occasionally. If this problem is severe, a tracking system should be included in the instrument to keep it on target. Field studies to provide data on turbulence effects would make it possible to consider various means for reducing turbulence-induced degradation.

R. T. MENZIES
M. S. SHUMATE
Jet Propulsion Laboratory, California Institute of Technology, Pasadena

Table 1. Experimental sensitivities to pollutant gases. The gases were at 298 K, except for NO, which was at 390 K. The band designations I and II refer to the upper and lower of the two mixed (10^00, 02^00) states.

Gas	Sensitivity (atm cm)	Laser line	Wavelength (μm)
Nitric oxide	10^{-2}	$^{12}C^{16}O$: 7–6, $P(15)$	5.19
Sulfur dioxide	10^{-2}	$^{12}C^{18}O_2$: 00^01–II, $R(40)$	9.02
Ozone	2×10^{-4}	$^{12}C^{18}O_2$: 00^01–II, $P(40)$	9.50
	2×10^{-4}	$^{12}C^{16}O_2$: 00^01–II, $P(14)$	9.50
Ethylene	5×10^{-5}	$^{12}C^{16}O_2$: 00^01–I, $P(14)$	10.53
Ammonia	10^{-4}	$^{12}C^{16}O_2$: 00^01–I, $P(32)$	10.72

References and Notes

1. R. T. Menzies, *Appl. Phys. Lett.* **22**, 592 (1973).
2. E. D. Hinkley and P. L. Kelley, *Science* **171**, 635 (1971); E. D. Hinkley, *Opto-Electronics* **4**, 69 (1972).
3. R. T. Menzies, *Appl. Opt.* **10**, 1532 (1971); *Opto-Electronics* **4**, 179 (1972).
4. R. H. Dicke, *Rev. Sci. Instrum.* **17**, 268 (1946).
5. J. H. McElroy, *Appl. Opt.* **11**, 1619 (1972).
6. P. Brockman and R. K. Seals, Jr., paper L-8814, and R. K. Seals, Jr., paper L-8866, presented at the Sixth Fluid and Plasma Dynamics Conference of the American Institute of Aeronautics and Astronautics, Palm Springs, Calif., July 1973.
7. D. L. Fried, *Proc. IEEE* (*Inst. Electr. Electron. Eng.*) **55**, 57 (1967).

8. Supported by NASA contract NAS 7-100.

5 December 1973; revised 11 January 1974

Brain Capillary Blockage Produced by a Virulent Strain of Rodent Malaria

Abstract. *A sudden enhancement in virulence of a mild* Plasmodium berghei yoelii 17 x *strain resulted in fulminating and fatal infections in CF1 and A/J mice. The virulent strain has maintained its characteristics after ten cyclical transmissions through* Anopheles stephensi. *The visible expression of virulence of the mutated strain is its ability to cross the blood-brain barrier and cause intravascular sequestration of injected erythrocytes and blockage of brain capillaries. We, therefore, believe that the virulent line of* Plasmodium berghei yoelii 17 x *could serve as a useful laboratory model for the study of "cerebral malaria."*

Obstruction of brain capillaries by parasitized erythrocytes occurs in falciparum (malignant tertian) malaria of man and can lead to death. Consequently, "cerebral malaria" has been studied both clinically and histologically since the early part of this century (*1*). Recently, attempts have been made to discover the causes of intravascular sequestration of infected erythrocytes in primate malaria models, such as, *Plasmodium knowlesi* and *P. coatneyi* in rhesus monkeys (*Macaca mulatta*) and *P. falciparum* in the night monkey (*Aotus trivigatus*) (*2*).

The findings of these investigations have clarified some of the mechanisms of intravascular sequestration and the changes in parasitized erythrocytes which enhance their ability to adhere and subsequently block the lumen of capillaries. These studies have also revealed the early and late sites of vascular schizogony in other organs. The pathological process involved, according to Maegraith (*3*), is stasis and loss of fluids and proteins which lead to cytotoxic anoxemia.

Rudzinska and Trager reported changes in the fine structure of infected erythrocytes (*4*), and Miller reported a decrease in the deformability of these cells (*5*). The different sites and organs of deep vascular schizogony early in the infection were demonstrated for *P. knowlesi*, *P. coatneyi*, and *P. falciparum* in their experimental primate hosts (*6*). However, there is no cerebral involvement in any of these infections in spite of the very high parasitemias. The histopathological picture of "cerebral malaria" in fatal cases of *P. falciparum* infections in man has not been observed in any other mammalian plasmodial infection.

We have discovered a suitable laboratory model for the study of brain involvement and cerebral capillary blockage in malaria infection. *Plasmodium berghei yoelii 17 x* normally causes an infection which is low in parasitemia and mild in its course. A strain of this plasmodium underwent an enhancement in virulence after its removal from our deep freeze. This virulent line caused fulminating and fatal infections in CF1 and A/J mice within 6 to 7 days after intraperitoneal injection of 10^6 parasitized erythrocytes. Parasitemia rose rapidly and reached 71 to 85 percent in the terminal phase of the infection. The virulent line of *P. b. yoelii* maintained its virulence during ten cyclical transmissions through *Anopheles stephensi* and 28 blood transfers. Its enzyme patterns were the same as that of the mild parent strain (*7*). Mice which recover from the mild *P. b. yoelii 17 x* were immune to the virulent *P. b. yoelii 17 x* line (*8*).

This enhanced virulence appears to involve the brains of the infected mice. Fine petechial hemorrhages were seen on the surface and in sections of the brain. Blockage of brain capillaries by infected erythrocytes were observed in brain smears stained in Giemsa (brain squash preparations), and 10 to 20 percent of the capillaries which we counted were affected. Both the fine capillaries which permit the passage of a single red cell and wider capillaries (Fig. 1, A, B, and C) were involved. The various stages of schizogonic development could be seen in the adhering, infected cells. "Ballooning" and aneurism formations in blocked capillaries were often observed (Fig. 1D). The ballooned areas were packed with infected erythrocytes and pigment. The cause and mechanism of the ballooning within the capillaries have not yet been determined. Twenty-two of 24 CF1 mice infected with the virulent line of *P. b. yoelii 17 x* showed this involvement of the brain capillaries. In a more recent experiment, eight CF1 mice and four

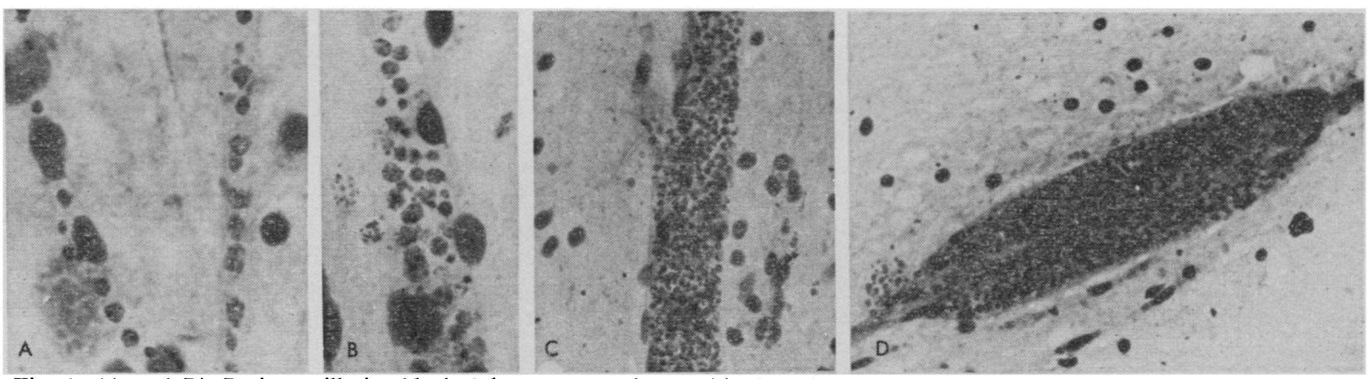

Fig. 1. (A and B) Brain capillaries blocked by sequestered, parasitized erythrocytes. Parasites are in different stages of their schizogonic development (brain smear stained in Giesma; × 960). (C) Large brain capillary blocked by sequestered, parasitized erythrocytes (Giemsa; × 420). (D) "Ballooning" in a brain capillary packed with parasitized erythrocytes (Giemsa; × 420).